2018 18th International Conference on Control, Automation and Systems (ICCAS 2018)
Oct. 17–20, 2018; YongPyong Resort, PyeongChang, GangWon, Korea

Combined Stiffness Identification of 6-DoF Industrial Robot

Kai Egil Berntsen[1], André Bleie Bertheussen[1] and Ilya Tyapin[1*]

[1]Department of Engineering and Science, University of Agder,
Grimstad, Norway (ilya.tyapin(at)uia.no) * Corresponding author

Abstract: In this paper a new combined local/global approach for estimating the combined stiffnesses of joints in anthropomorphic robots is presented. The stiffness of each joint is a combination of several effects: i) stiffness of the links, ii) stiffness of joint bearings and gears and iii) stiffness of the position control loops given by the individual axis controller gains in the controller software. Experimental results are presented for an ABB IRB6600 industrial robot using measurements from a FARO Xi laser tracker and an ATI Omega160 force/torque sensor. The results show that there is a significant variation in stiffness among the individual joints of the robot and that the stiffnesses of the main axes (1-3) are significantly higher than the stiffnesses of the wrist axes (4-6). The results presented in this paper are valid in the home position of the robot, but the method can be modified and used for any robot position. The method requires much less experimental data compared to a global approach. In order to see the impact of pre-loading the joints in the joint stiffness analysis an experiment was conducted on joint 1. The influence of complementary stiffness matrix $\mathbf{K_c}$ on Cartesian stifness matrix $\mathbf{K_x}$ is also evaluated in this paper.

Keywords: 6 DoF Industrial Robot, Joint Stiffness Identification, Complimentary Stiffness Matrix.

1. INTRODUCTION

The application of industrial robots in high-precision contact applications such as machining operations has received significant interest in recent year. One example of development in this area has been the automatic generation of 3- and 5-axis toolpaths from CAD/CAM software to robot programs. One weakness of CAD/CAM-based off-line programming of industrial robots is potentially large deflections of the robot arm compared to traditional CNC machines. Deflections can be in the order of several millimeters and must be taken into account if industrial robots are applied to the machining of hard materials, but also of soft materials when high material removal rates are required.

Deflections of industrial arms when used in contact applications have several causes: i) compliance of the links, ii) compliance of joint bearings and gears and iii) compliance of the position control loops which are typically influenced by the individual axis controller gains in the controller software. One possible approach to increase the accuracy of robotic machining is to adjust the off-line generated CAD/CAM-based toolpaths based on estimates of the robot's joint stiffnesses and estimated or measured forces from the machining operations.

In order to make such adjustments, accurate estimates of the robot's combined joint stiffnesses are key parameters in addition to the process model, see for example [1]. In [1] a similar method for identifying the joint stiffness of six-revolute industrial serial robots was presented. A wrench (3 forces and 3 torques) was applied to the end-effector and the end-effector displacements were measured. A pseudo-inverse approach was used to identify the joint stiffnesses. The joint stiffnesses were estimated in robot positions where the complementary stiffness matrix $\mathbf{K}_c$ (see [2] for the definition) was negligible. In [3] it is assumed that the first three joints have the largest impact on the end effector position, and the stiffness is calculated for these joints based on given data for motors and gears. Another method described in [4] is to clamp all the joints except for the one evaluated, and evaluate the stiffness individually. The process is repeated for all the joints. Joint stiffness are identified by the clamping method, where the robot is locked in a closed kinematic loop and then exercises joint-based movements while sensing motor position and torque in [5].

The method presented in this paper differs to [1] and [3] in the following: i) the stiffness of several individual joints are estimated independently from each other as opposed to a global approach using the pseudo-inverse, ii) the laser tracker reflector is moved to strategic locations to measure deflections not only at the tool-center-point (TCP) and iii) joints are not clamped. Similar to [1] it is assumed that the effects from the complementary stiffness matrix $\mathbf{K}_c$ can be neglected. To minimize potential effects of $\mathbf{K}_c$ relatively small forces were applied on the TCP (less than 250N). The estimated stiffness values contain the combined compliance effects of links, bearings, gears and controller gains. In this paper joint configurations are chosen to acquire a high degree of isolation for the evaluated joint. Another way to isolate a joint is to use several reflector positions and do measurements on both sides of a joint with the robot both loaded and unloaded. This approach is used in the evaluation of joints 4 and 5. In addition, the force used to evaluate joint 2 is attached directly in joint 3, in order to eliminate any contribution from joint 3.

The paper is organised as follows: in Section 2 the experimental setup is presented, Section 3 presents the proposed robot stiffness identification method. Section 4 presents an influence of complimentary stiffness ma-

trix on Cartesian stiffness. In Section 5 the results are presented followed by an evaluation of the influence of pre-loading the joints in the stiffness analysis, while conclusions and discussion are given in Section 6.

2. ROBOT KINEMATICS AND EXPERIMENTAL SETUP

The experimental setup is composed of a robot (ABB IRB6600-2.55m-175kg), FARO Xi laser tracker and a reflector with a typical measurement accuracy of $10 - 30\mu m$. The force applied to the end-effector is measured by an ATI Omega160 6DoF force/torque sensor with a measurement accuracy of $0.25 - 0.5N$ connected to the robot's mounting flange. The robot kinematic model, coordinate systems and D-H parameters used in this paper are shown in Fig. 1 and Table 1, where the global coordinate system, each joint coordinate system and the coordinate system related to ATI Omega160 6DoF force/torque sensor are shown in Fig. 1. The red circles represent FARO Xi laser tracker reflector positions used during the joint stiffness identification. In order to reduce the measurement noise, the forces are applied using a rope, pulley and external load, instead of being manually applied. The external load used for all stiffness identification experiments has a weight of $20.120kg$.

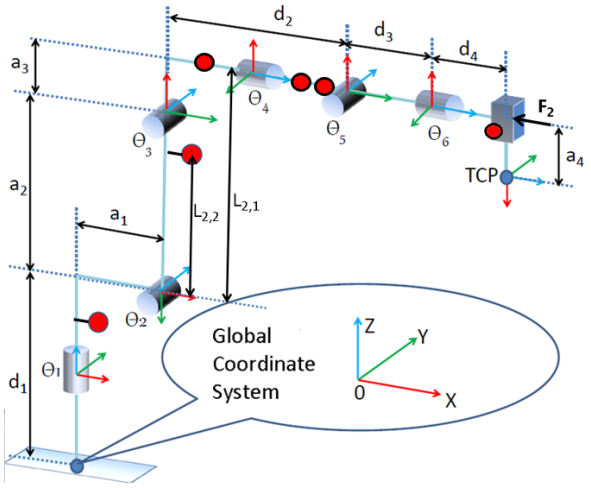

Fig. 1 *Illustration of coordinate system and robot kinematic parameters.*

Table 1 *D-H parameters.*

#	θ, (rad)	d, (mm)	a, (mm)	α, (rad)
1	θ_1	d_1, (780)	a_1, (320)	$-\frac{\pi}{2}$
2	$\theta_2 - \frac{\pi}{2}$	0	a_2, (1075)	0
3	θ_3	0	a_3, (200)	$-\frac{\pi}{2}$
4	θ_4	d_2, (1142)	0	$\frac{\pi}{2}$
5	$\theta_5 + \frac{\pi}{2}$	0	0	$-\frac{\pi}{2}$
6	$\theta + \pi$	$d_3 + d_4$, (380)	a_4, (0)	0

3. STIFFNESS IDENTIFICATION

The methods used to identify joint stiffness of robots can be classified in two categories: global and local. The global method is based on measurements at the end-effector TCP position. In the global approach the external force **F** is measured by a force sensor while the TCP position and orientation are measured by an external 3D measurements system. The advantage of this method is the easiness of installation, since the experimental setup remains the same for all measurements. However, the results depend on the robot's configuration, the position measurements include the link deformations and the identification quality depends on a number of parameters to be identified at the same time.

Local methods identify only one joint stiffness at the time. However these methods may require the robot to be disassembled for accurate results. The proposed approach combines both local and global methods and is conducted with the robot in home position, as defined in Fig. 1 and Table 1 with changes in configuration summarised in Table 2. In order to include the controller gains into the analysis, the joint brakes are released and the joints are pre-loaded. In the experiments, except the evaluation of joint 2, where the force is applied directly to the joint 3, the external force is applied to the end effector.

Table 2 *Joint Angles used for Stiffness Identification. The second column shows a difference from home position*

Identified Joint	Rotation, (rad)
q_1	–
q_2	$q_3 = -\frac{\pi}{6}$
q_3	$q_5 = \frac{\pi}{2}$
q_4	$q_4 = \frac{\pi}{2}$, $q_5 = -\frac{\pi}{2}$ and $q_6 = \frac{\pi}{2}$
q_5	–
q_6	$q_5 = \frac{\pi}{2}$

Joint 1. The stiffness of joint 1 is identified by measuring the local joint displacement while the external force is applied to the spindle in the global Y-direction. The reflector is placed on the robot base as shown in Fig. 2. The reflector position is measured using the Faro Xi laser tracker and the applied load is measured by the ATI Omega 160. The first joint stiffness is found in Eq. 1.

$$K_1 = \frac{F_{l1} \cdot L_{11} \cdot L_{21}}{L_1} \quad (1)$$

$$L_1 = \sqrt{(x - x_0)^2 + (y - y_0)^2 + (z - z_0)^2} \quad (2)$$

where F_{l1} is the external force, L_{11} is the moment arm of the applied load, L_{21} is the distance from joint 1 to the reflector position, x, y, z are reflector coordinates measured by laser tracker, x_0, y_0, z_0 are reflector coordinates measured by laser tracker before the external force is applied.

Joint 2. The stiffness of joint 2 is also identified by measuring the local joint displacement while the exter-

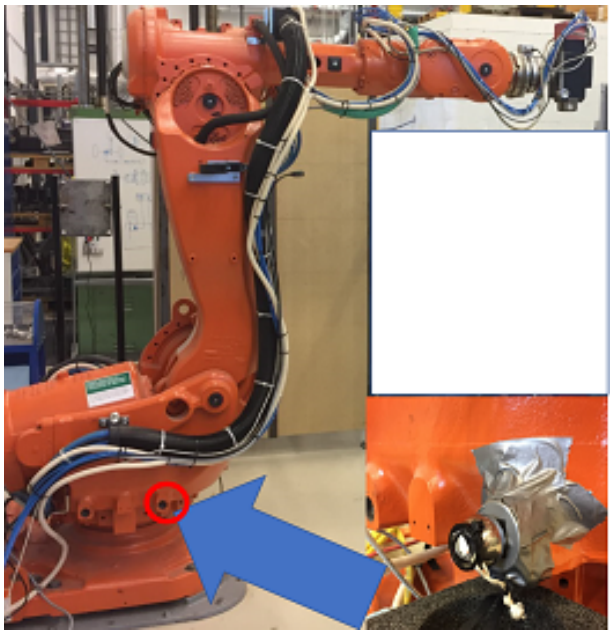

Fig. 2 *Stiffness Identification Joint 1. Reflector Location*

nal force is applied in the global X-direction. A reflector is placed on the robot in the "joint 3 ring" as shown in Fig. 3. The external force is applied directly to the joint 3 and it is connected directly to the robot using a rope and pulley. The second joint stiffness is identified using the same equations as the first joint stiffness, where the external force, the moment arm of the applied load and the distance from the joint to the reflector position are different.

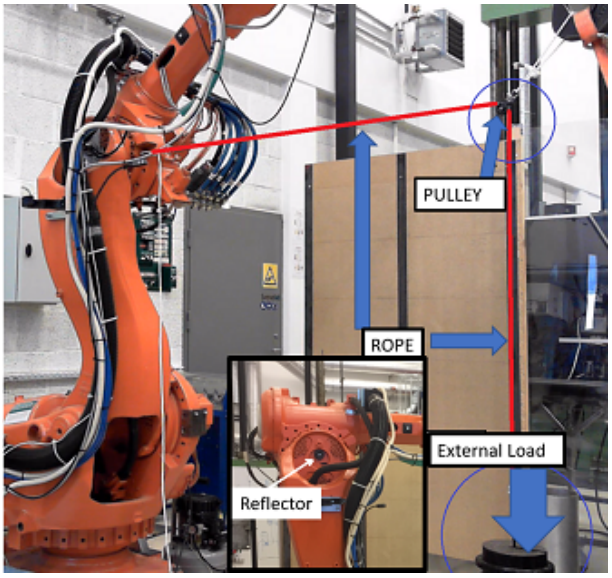

Fig. 3 *Stiffness Identification Joint 2. Reflector Location. Rope and Pulley Setup.*

Joint 3. The approach to identify the stiffness of joint 3 is a combination of local and global methods. A reflector is placed on the robot spindle as shown in Fig. 4.

A force is applied to the spindle in the global negative Z-direction. In addition, the applied load will also cause a small angular deflection in joint 2. Since the stiffness of joint 2 is identified, it can be subtracted from the laser tracker measurements and the joint 3 stiffness is found in Eq. 3.

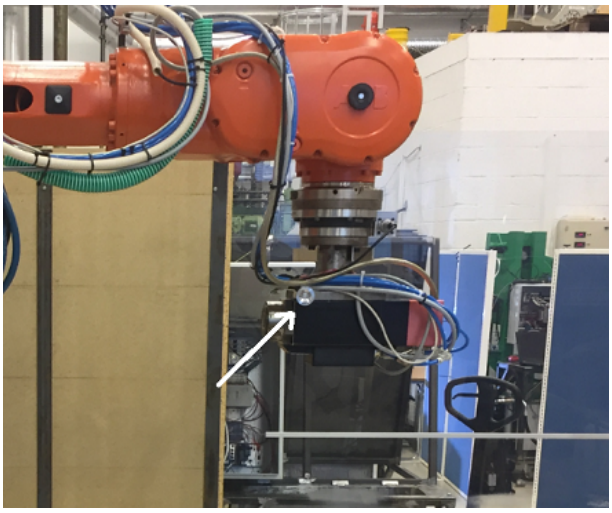

Fig. 4 *Stiffness Identification Joint 3. Reflector Location.*

$$K_3 = \frac{F_{l3} \cdot L_{13} \cdot L_{23}}{L_3} \quad (3)$$

$$L_3 = \sqrt{(x-x_0-d_{2,x})^2+(y-y_0-d_{2,y})^2+(z-z_0-d_{2,z})^2}$$

$$\mathbf{d_2} = \mathbf{J} \cdot [\mathbf{0} \quad \frac{\tau_\mathbf{2}}{\mathbf{K_2}} \quad \mathbf{0} \quad \mathbf{0} \quad \mathbf{0} \quad \mathbf{0}]^\mathbf{T} \quad (4)$$

$$\tau = \mathbf{J} \cdot \mathbf{W}$$

where L_{13} is the moment arm of the applied load, L_{23} is the distance from joint 3 to the reflector position, $\mathbf{d_2}$ is the displacement caused by the second joint, τ is the torque vector, $\mathbf{J}$ is the robot Jacobian matrix, $\mathbf{W}$ is the wrench from the ATI Omega 160 force sensor.

Joint 4. To identify the stiffness of joint 4, the reflector is placed on each side of the joint, *A* and *B*, as shown in figure 5. The external force is applied to the spindle in the global negative Z-direction. In addition, the applied load will also cause a small angular deflection in joints 2 and 3. The contribution from joint 2 and 3 is included into the estimation of joint 4 stiffness. Vectors from point *A* to point *B* and their lengths for loaded (external force is applied) and unloaded robot are found in Eqs.5-8. The fourth joint stiffness is found in Eq.11.

$$\mathbf{AB_u} = [(B_{x_0}-A_{x_0}) \quad (B_{y_0}-A_{y_0}) \quad (B_{z_0}-A_{z_0})] \quad (5)$$

$$\mathbf{AB_l} = [(B_x - A_x) \quad (B_y - A_y) \quad (B_z - A_z)] \quad (6)$$

$$|\mathbf{AB_u}| = \sqrt{(AB_{u,x})^2 + (AB_{u,y})^2 + (AB_{u,z})^2} \quad (7)$$

$$|\mathbf{AB_l}| = \sqrt{(AB_{l,x})^2 + (AB_{l,y})^2 + (AB_{l,z})^2} \quad (8)$$

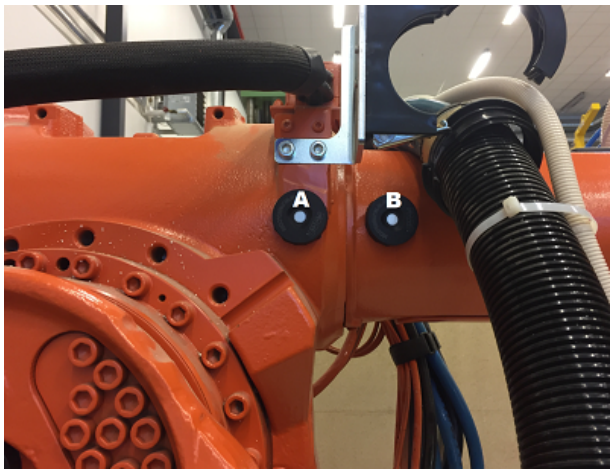

Fig. 5 *Stiffness Identification Joint 4. Reflector Locations.*

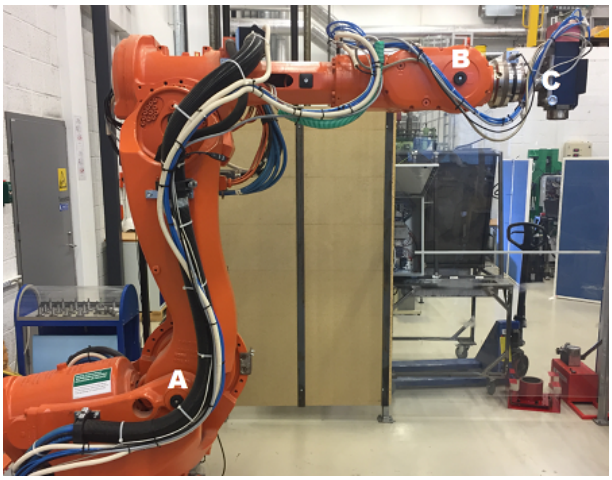

Fig. 6 *Stiffness Identification Joint 5. Reflector Locations.*

The angle ϕ between vectors $\mathbf{AB_u}$ and $\mathbf{AB_l}$ is found in Eq. 9. The contribution (α) of joints 2 and 3 to the angle ϕ is found in Eq. 10:

$$\phi = cos^{-1}\left(\frac{\mathbf{AB_u}\cdot\mathbf{AB_l}}{|\mathbf{AB_u}|\cdot|\mathbf{AB_l}|}\right) \quad (9)$$

$$\alpha = \left|tan^{-1}\left(\frac{\sqrt{(A_x-A_{x_0})^2+(A_y-A_{y_0})^2+(A_z-A_{z_0})^2}}{L_{24}}\right)\right| \quad (10)$$

$$K_4 = \frac{F_{l4}\cdot L_{14}}{\theta_4} \quad (11)$$

The angular displacement θ_4 in joint 4 is found in Eq. 12:

$$\theta_4 = tan^{-1}\left(\frac{|\mathbf{AB_u}|\cdot\mathbf{tan}(\phi-\alpha)}{R_4}\right) \quad (12)$$

where L_{14} is the moment arm of the applied load, L_{24} is the distance from joint 3 to the reflector position *A*, R_4 is the radius from the fourth joint origin to the reflector position *B*.

Joint 5. The approach to measure the local angular deflection in the joint is used to identify the stiffness in joint 5. Three reflector pucks are placed on the robot, *A*, *B* and *C*, as shown in Fig. 6. Positions are measured by the laser tracker while the reflector attached to all three pucks alternately. The measurements are done while the robot is unloaded and loaded. The external force is applied to the spindle in the global negative Z-direction. In addition, a contribution of joints 2 and 3, is considered to identify the stiffness of joint 5. The vectors connecting points *A*, *B*, and *B*, *C*, while the robot is loaded and unloaded are found in Eqs. 13-16.

$$\mathbf{AB_u} = [(B_{x_0}-A_{x_0}) \quad (B_{y_0}-A_{y_0}) \quad (B_{z_0}-A_{z_0})] \quad (13)$$

$$\mathbf{AB_l} = [(B_x-A_x) \quad (B_y-A_y) \quad (B_z-A_z)] \quad (14)$$

$$\mathbf{BC_u} = [(C_{x_0}-B_{x_0}) \quad (C_{y_0}-B_{y_0}) \quad (C_{z_0}-B_{z_0})] \quad (15)$$

$$\mathbf{BC_l} = [(C_x-B_x) \quad (C_y-B_y) \quad (C_z-B_z)] \quad (16)$$

The angular difference between $\mathbf{AB}$ and $\mathbf{BC}$ is calculated in Eqs. 17-18

$$\phi_u = cos^{-1}\left(\frac{\mathbf{AB_u}\cdot\mathbf{BC_u}}{|\mathbf{AB_u}|\cdot|\mathbf{BC_u}|}\right) \quad (17)$$

$$\phi_l = cos^{-1}\left(\frac{\mathbf{AB_l}\cdot\mathbf{BC_l}}{|\mathbf{AB_l}|\cdot|\mathbf{BC_l}|}\right) \quad (18)$$

The angular displacement (θ_5) of joint 5 as a result of the applied load is found in Eq. 19 and the stiffness of joint 5 (K_5) is found in Eq. 20

$$\theta_5 = \phi_l - \phi_u \quad (19)$$

$$K_5 = \frac{F_{l5}\cdot L_{15}}{\theta_5} \quad (20)$$

where L_{15} is the moment arm of the applied load.

Joint 6. The stiffness of joint 6 is identified in a similar manner as the stiffness of joint 3. A reflector is placed on the spindle as shown in figure 4. The external force is applied to the end effector in the global Y-direction through an external link mounted on the tool. The applied load creates a torque in joint 6 which is measured by ATI Omega 160 force/torque sensor. The deflection caused by joint 1 is considered and subtracted from the laser tracker measurements. The stiffness of joint 6 is found in Eq. 21.

$$K_6 = \frac{F_{l6}\cdot L_{16}\cdot L_{26}}{L_6} \quad (21)$$

$$L_6 = \sqrt{(x-x_0-d_{1,x})^2+(y-y_0-d_{1,y})^2+(z-z_0-d_{1,z})^2} \quad (22)$$

$$\mathbf{d_1} = \mathbf{J}*[\frac{\tau_1}{\mathbf{K_1}} \quad \mathbf{0} \quad \mathbf{0} \quad \mathbf{0} \quad \mathbf{0} \quad \mathbf{0}]^{\mathbf{T}} \quad (23)$$

$$\tau = \mathbf{J}*\mathbf{W} \quad (24)$$

where L_{16} is the moment arm of the applied load, L_{26} is the distance from joint 6 to reflector position, $\mathbf{d_1}$ is the displacement caused by joint 1, τ is the torque vector, $\mathbf{J}$

is the robot Jacobian matrix, $\mathbf{W}$ is the wrench from ATI Omega 160 sensor.

4. INFLUENCE OF COMPLIMENTARY STIFFNESS MATRIX

The Cartesian stiffness matrix ($\mathbf{K_x}$) including complementary stiffness matrix ($\mathbf{K_c}$) and the joint stiffness matrix ($\mathbf{K}_\theta$) is presented in [1] and Eq. 25. If the influence of $\mathbf{K_c}$ is small and can be neglected, Eq. 25 is reduced to Eq. 26.

$$\mathbf{K_x} = \mathbf{J^{-T}} \cdot (\mathbf{K}_\theta - \mathbf{K_c}) \cdot \mathbf{J^{-1}} \quad (25)$$

$$\mathbf{K_x} \approx \mathbf{J^{-T}} \cdot \mathbf{K}_\theta \cdot \mathbf{J^{-1}} \quad (26)$$

If complimentary stiffness matrix is assumed to be equal zero, only joint stiffness identification is needed. In order to investigate the influence of $\mathbf{K_c}$ on $\mathbf{K_x}$, and to determine when $\mathbf{K_c}$ can be neglected, an calculation routine is performed. The difference in displacement of the robot end-effector pose when $\mathbf{K_c}$ is null and not null is investigated for different configurations of the robot when subjected to a load. Two ratios ν_p and ν_r in Eqs. 27-28 are defined and used to analyse the influence of the complementary stiffness matrix ($\mathbf{K_c}$) on the position and rotation displacements respectively.

$$\nu_p = \frac{|\delta p_{\mathbf{K_c}} - \delta p_{\mathbf{K_c 0}}|}{max(\delta p_{\mathbf{K_c}}, \delta p_{\mathbf{K_c 0}})} \quad (27)$$

$$\nu_r = max \left\{ \begin{array}{l} |\delta r_{x\mathbf{K_c}} - \delta r_{x\mathbf{K_c 0}}| \\ |\delta r_{y\mathbf{K_c}} - \delta r_{y\mathbf{K_c 0}}| \\ |\delta r_{z\mathbf{K_c}} - \delta r_{z\mathbf{K_c 0}}| \end{array} \right\} \quad (28)$$

where $\delta p_{\mathbf{K_c}}$ is the displacement of the robot end-effector, $\delta p_{\mathbf{K_c 0}}$ is the displacement of the robot end-effector when $\mathbf{K_c}$ is null, $(\delta r_{x\mathbf{K_c}}, \delta r_{y\mathbf{K_c}}, \delta r_{z\mathbf{K_c}})$ is the angular displacement of end-effector about x_0,y_0, z_0, $(\delta r_{x\mathbf{K_c 0}}, \delta r_{y\mathbf{K_c 0}}, \delta r_{z\mathbf{K_c 0}})$ is the angular displacement of end-effector about x_0,y_0 and z_0 when $\mathbf{K_c}$ is null.

As joints 2 and 3 are the joints that contribute most to translational motion [3] of the end-effector, these joints are variables in the calculation. Joint 1 has no influence and is set to 0. Joints 4, 5 and 6, contribute primarily to the end effector orientation, and are set to $\frac{\pi}{4}$ radians in order to keep the wrist configuration far from singularities [1]. Results from the performed joint stiffness analysis are used to generate $\mathbf{K}_\theta$. Joint 2 ranges from $-65°$ to $75°$ and joint 3 ranges from $-180°$ to $60°$ are used in simulations. The wrench containing forces and moments $\mathbf{W_{load}}$ is set to $[200N\ 200N\ -2500N\ 0Nm\ 0Nm\ 0Nm]$.

5. RESULTS

The results from the joint stiffness identification experiments are presented in Table 3. The results are normalised to the highest stiffness of joint 1. A static load was used in experiments and position measurements were recorded by Faro laser tracker. Each experiment is divided into two parts: 1) record the reflector position before the load is applied, 2) record the reflector position after applying the external load. The results are calculated using mean values from both the ATI Omega force sensor, and the Faro laser tracker.

Table 3 *Identified Joint Stiffness Normalized to Joint 1.*

J 1	J 2	J 3	J 4	J 5	J 6
1	0.887	0.6892	0.141	0.048	0.0187

In order to see the impact of pre-loading the joints in the joint stiffness analyses an additional experiment was conducted on joint 1. The reason for this experiment is to evaluate the influence of back-lash in the test. The results of this experiment are shown in table 4, where they are also normalised to the highest stiffness (joint 1) in the complete stiffness analysis in Table 3. The pre-loaded joint 1 is investigated in $Case$ 1, where the joint 1 is jogged to one side and the external load is applied in the same direction as the robot movement. The non-loaded joint 1 is investigated in $Case$ 2, the external load is applied in the opposite direction to the robot movement and gearbox backlash is taken into account. A deviation in identified stiffness is 24 $\%$ and this effect has to be considered in a path planning routine.

Table 4 *Stiffness of Joint 1. Pre-loaded and Non-loaded.*

	Case 1	Case 2
J.S.	1.015	0.758

The ratios ν_p and ν_r are calculated for all values within the range of joints 2 and 3 to investigate if the complementary stiffness matrix ($\mathbf{K_c}$) has any influence on the Cartesian stiffness matrix ($\mathbf{K_x}$). This is done to evaluate if $\mathbf{K_c}$ can be neglected when evaluating the robot stiffness. The contour plot in figure 7 shows that there are robot configurations where $\mathbf{K_c}$ influences on $\mathbf{K_x}$ in position. The dark blue colour indicates no influence and the light green colour shows regions where the influence is higher. The highest value is $\nu_p \leq 9.42 \cdot 10^{-4}$m for the wrench $[200N\ 200N\ -2500N\ 0Nm\ 00Nm\ 0Nm]$ and the results are suitable for many operations including machining where industrial robots are used.

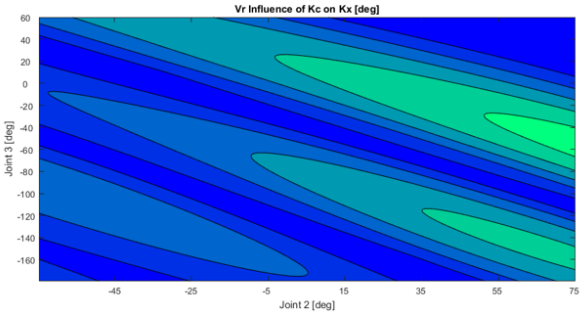

Fig. 7 *Influence of* $\mathbf{K_c}$ *on* $\mathbf{K_x}$ *in Position.*

6. CONCLUSIONS

A joint stiffness analysis was conducted on the ABB IRB 6600 industrial manipulator. The results are not given directly in this paper, as they are considered to be a sensitive information. Hence, the presented results are normalised relative to joint 1.

The stiffness analysis for joint 1 includes the base, motor, gearbox and controller. The stiffness identification of joint 2 includes the link between joint 2 and 3, motor, controller and gearbox. In addition, the load was attached directly to joint 3 to isolate joint 2. The analysis of joint 3 includes the links between joints 3 and 5, motor with controller, and gearbox. However, the applied load causes a deflection in joint 2. This deflection is included into the stiffness estimation of joint 3. To analyse the stiffness in joint 4 and 5, the local angular deflection in the respective joint is measured. For both of these analyses, the applied load causes a deflection in joints 2 and 3, which influence the total measured displacement. This is compensated by calculating the angle for the evaluated joint before and after applying the load. When the stiffness in joint 6 was evaluated, an external link was mounted in order to create a moment in the joint. The load applied to the link causes a displacement in joint 1, which influence the total measured displacement. This is included in the evaluation of joint 6.

One benefit of the proposed method is the fact that the stiffness of individual joints (1,2,4,5) are estimated independently of other joints. The estimated stiffness of joints 3 and 6 require knowledge of stiffnesses estimated in previous steps. By estimating joints individually, much fewer experiments are needed. When using the pseudo-inverse global approach, one must always ensure that the system identification problem is persistently excitated and that the matrix which must be pseudo-inverted has a good condition number. These considerations usually require a much larger set of experimental data compared to the method presented in this paper.

The estimated joint stiffnesses include several effects such as stiffnesses in bearings, gears, links and controller gains. It is these overall stiffness values which are of interest when developing machine-dependent compensation methods for off-line-generated toolpaths. The stiffness of a manipulator depends on the configuration, hence the stiffness could be found in different configurations and interpolation techniques could be used to compute the stiffness in all other configurations.

The conducted experiments regarding pre-loading of the joints show that there is a vast difference between pre-loaded and non-loaded joints. Therefore, in the conducted joint stiffness identification, all 6 joint were intentionally pre-loaded after releasing the brakes. The results can therefore be used for all joints, as long as the joints are considered pre-loaded. Once the joint changes a direction of rotation during a machining process, for example, it is considered as non-loaded.

The influence of complementary stiffness matrix $\mathbf{K_c}$ on Cartesian stifness matrix $\mathbf{K_x}$ is also evaluated. The result show that there are regions where $\mathbf{K_c}$ has minor influence. The wrench used to evaluate the influence also contains forces substantially larger than the forces required for many machining operations. Therefore it was assumed that the complementary stiffness matrix could be neglected in many cases where an industrial robots are used. However, it has to be considered while hard material machining operations.

REFERENCES

[1] C. Dumas and S. Caro and S Garnier and B. Furet, "Joint Stiffness Identification of Six-Revolute Industrial Serial Robots", *Robotics and Computer-Integrated Manufacturing*, vol 27, pp. 881-888, 2011.

[2] S.-F. Chen and I. Kao, "Conservative congruence transformation for joint and Cartesian stiffness matrices of robotic hands and fingers", *International Journal of Robotics Research*, vol 19, pp. 835-847, 2000.

[3] S. Chen and T. Zhang and M. Shao, "A 6-DOF Articulated Robot Stiffness Research", *12th World Congress on Intelligent Control and Automation (WCICA)*, pp. 3230-3235, 2016.

[4] E. Abele and M. Weigold and S. Rothenbucher, "Modeling and Identification of an Industrial Robot for Machining Applications", *Manufacturing Technology*, Elsevier, vol 56(1), 2007.

[5] M. Haage, M. Halbauer, C. Lehmann, J.P. Staedter, "Increasing Robotic Machining Accuracy Using Offline Compensation Based on Joint-Motion Simulation", *In Proceedings of the 41st International Symposium on Robotics (ISR/Robotik 2014)*, pp. 18, 2014.